A facile metal-phenolic-amine strategy for dual-functionalization of blood-contacting devices with antibacterial and anticoagulant properties†

Abstract: Thrombosis and infections of extracorporeal circuits and indwelled medical devices are the two major life-threatening complications faced in clinical practice. Herein, we report a novel and facile metal-phenolic-amine surface modification strategy to engineer a multifunctional coating on these devices to combat thrombosis and infection. This strategy is inspired by the metal-catecholamine coordination complex of [Fe(dopa)$_3$] in mussels, in which Cu(II) ion (metal), plant polyphenol gallic acid (phenolic) and cystamine (amine) are employed to fabricate a copper-phenolic-amine network. Our *in vitro* and *in vivo* experiments reveal that the resultant Cu(II)-chelating coatings enable the modified tubing with not only durable antibacterial properties, but also capability to persistently generate anticoagulant therapeutic nitric oxide (NO) gas in the presense of endogenous S-nitrothiol (RSNO) from fresh blood. We anticipate that our simple and multifunctional coating strategy would be a milestone in the development of surface engineering, especially to that of biomedical devices.

1. Introduction

Thrombosis and infections, the two major clinical complications of indwelling medical devices and extracorporeal circuits, often lead to device failure, patient morbidity, mortality, and increased healthcare costs.[1-5] Co-administration of anticoagulant drugs (e.g., heparin) and antibiotics is a common strategy to reduce thrombosis and infections in clinical practice. However, this may lead to the development of heparin-induced thrombocytopenia (HIT) and other side effects like bleeding and bacterial resistance.[6-8] Moreover, administration of antibiotics may lead to fever, thrombophlebitis and epidermal necrolysis, which are unfavorable and much worse than infection itself.[9-10] Therefore, new therapeutic approaches to combat thrombosis as well as infections are highly sought after.

Surface modification strategies, including poly(ethylene glycol) (PEG) coating,[11] zwitterionic polymer grafting,[12] hyaluronic acid modification,[13] superhydrophobic[14] and bioinspired omniphobic surface treatment[15] have been shown to improve the antibacterial and anticoagulant properties of blood-contacting devices. Current coating technologies generally consist of tedious complicated processes including surface pretreatment of materials, chemical specificity between the material surface and the interfacial modifiers, and complex multistep procedures for anchoring bioactive molecules to the coatings. Thus, the development of a simple, efficient and versatile strategy to decorate extracorporeal circuits and indwelling medical devices with durable antithrombogenic and antiinfectious functions is indispensable in clinic.

Metal-phenolic surface chemistry inspired by the [Fe(dopa)$_3$] complexes to crosslink the protein mfp-1 in the byssus (Fig. 1A)[16] proves to be a promising surface coating strategy.[17] For example, metal-phenolic network (MPN) coatings like Fe^{III}-tannic acid (TA) (Fe^{III}-TA) coatings have been used as nanocoatings on many types of substrates like polystyrene (PS), poly(lactic-co-glycolic acid) (PLGA), melamine formaldehyde (MF), polydimethylsiloxane (PDMS), SiO_2 and Au.[17,18] However, in saline solutions, cations (particularly K^+) are easily adsorbed onto the substrate surfaces, forming a tightly bound hydration layer at the solid-liquid interface, weakening the phenolics to bind to the surfaces,[19-20] and resulting in unsuccessful MPN coating formation. As amine could help remove the hydrated salt layer from the surface for catechol binding, the adaptive synergy between the catechol and the amine (namely, catecholamine chemistry) has also been proposed to engineering surface coatings.[21]

Herein, co-inspired by metal-phenolic and catecholamine surface chemistry, we developed a biomimetic metal (Cu^{II})-phenolic (plant polyphenol gallic acid)-amine (cystamine) surface chemistry strategy to fabricate an advanced dual-functional coating by assembling mussel-inspired molecule/ion in a single step. In our design, the copper ions (Cu^{II}) are responsible for both the antibacterial[22-24] and antithrombotic properties[25] as they exhibit glutathione peroxidase (GPx)-like activity to produce the antithrombotic mediator nitric oxide (NO) from endogenous S-nitrosothiols (RSNO) in blood. Plant polyphenol gallic acid (GA) is selected due to its antibacterial, antiviral, and antiinflammatory properties (Fig. 1B). In addition, cystamine (CySA) is chosen to fabricate the metal-phenolic-amine-based coatings through phenolic-amine (GA-

CySA) molecularly assembled crosslinking and metal ion-polyphenol (Cu^{II}-GA) coordination bonding in the synergistic processes (Fig. 1C). After a simple dip-coating process, the robust chelation of a minute amount of Cu^{II} in the metal-phenolic-amine network endows the coated polyvinyl chloride (PVC) tubing with durable and significant antibacterial and antithrombogenic properties. We envision that our simple and multifunctional copper-phenolic-amine coating strategy will find wide applications in surface engineering of indwelled blood-contacting devices in clinic.

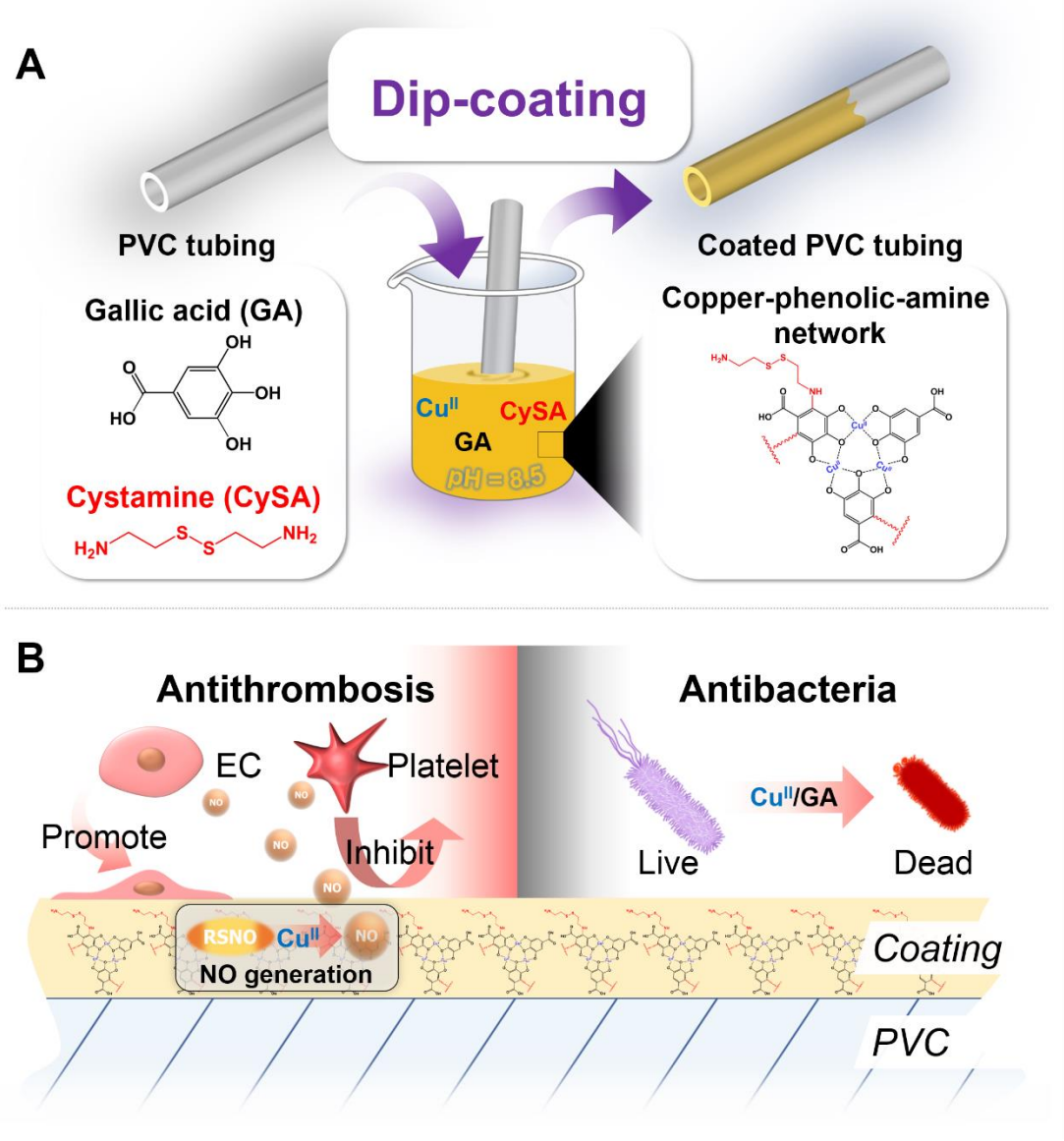

Fig. 1 Schematic diagram for the preparation of dual-function Cu^{II}-GA/CySA coating. (A) The facile metal-phenolic-amine surface chemistry strategy to fabricate the coating by dip-coating of PVC tubing in an alkaline mixture solution (pH 8.5) containing Cu^{II},

GA and CySA. (B) Such surface coating with copper-phenolic-amine network can confer the PVC tubing with the dual function of long-term antithrombosis and antibacteria. In this coating, Cu^{2+} with GPx-like catalytic activity is able to achieve antithrombotic property by generating anticoagulant therapeutic NO gas from RSNOs. On the other hand, GA and Cu^{2+} in the copper-phenolic-amine network can simultaneously bring synergistic inhibitory action to the bacterium growth.

2. Experimental Section

Preparation of the Cu^{II}-GA/CySA coatings

To prepare Cu^{II}-GA/CySA coatings, GA (0.5 mg/mL) and CySA (0.6 mg/mL) were dissolved in 10 mM Tris-HCl buffer (pH 8.5). Then, we added 0, 10, 20, 40 and 60 μg/mL feed concentrations of $CuCl_2 \cdot 2H_2O$, and soaked the planar PVC substrates in each of the mixed solutions. After 12 hours of immersion, the planar PVC substrates were ultrasonically cleansed with distilled water and dried with N_2. The Cu^{II}-GA/CySA-coated PVC substrates were marked as $Cu^{II}(0)$, $Cu^{II}(10)$, $Cu^{II}(20)$, $Cu^{II}(40)$ and $Cu^{II}(60)$ according to the feed concentrations of $CuCl_2 \cdot 2H_2O$ in the reaction system.

Characterization of the Cu^{II}-GA/CySA coatings

We used a field emission scanning electron microscopy (SEM, JSM-6390, JOEL, Japan) to analyze the surface morphology of the coating. Furthermore, silicon was used for the Cu^{II}-GA/CySA coatings deposition. We then applied a spectroscopic ellipsometer (M-2000V, J.A. Woollam, USA) and Cauchy model to measure the coating thickness.

We used a Krüss GmbH DSA 100 Mk 2 goniometer (Hamburg, Germany) to measure the water contact angle (WCA) of the coating at room temperature. Following that, a 5 μL of test liquid drop was used for image processing with DSA 1.8 software. There were a minimum of six values of WCA for each sample.

To analyze the chemical structure of the Cu^{II}-GA/CySA coatings, we used a Nicolet model 5700 instrument to take a Grazing incidence attenuated total reflection Fourier transform infrared (GATR-FTIR) spectrum.

An X-ray photoelectron spectroscopy (XPS) (XSAM200, Kratos Ltf, UK), supplied with a monochromatic A1 Kα (1486.6 eV); operated at 12 kV×15 mA and a pressure of 20 MPa, was utilized to analyze the surface elemental composition of the

Cu^{II}-GA/CySA coatings. With the use of 300 eV pass energy, we took the overview XPS spectra between 50 and 1300 eV with 0.5eV of energy step. We also recorded the detailed spectra of peaks of interests with a 0.05 eV energy step. Each sample had 15 min of total acquisiton time.

The measurement of Electron paramagnetic resonance (EPR) was performed by Bruker A320 equipped with Microwave Bridge to analyze the chelation of Cu^{II} to GA, in the resultant Cu^{II}-GA/CySA coatings. The detection parameters were set accordingly, 1×10^5 for the receiver gain, Gauss for modulation amplitude, 20 mW for microwave power, and 100 kHz for modulation frequency.

A MALDI micro MX time-of-flight mass spectrometer (Waters, Milford, MA), equipped with 337 nm N_2 laser operated with 4 ns-duration pulse, was utilized to perform Matrix assisted laser analysis of ionization spectrometry (MALDI-MS) measurement with reflection mode. The detailed operation and analysis were reported elsewhere.[26]

NO catalytic release detection

NO release induced by Cu^{II}-GA/CySA coating was monitored in real-time using a chemiluminescence NO analyzer (NOA) (Seivers 280i, Boulder, CO). The PVC substrate (0.5 cm × 1 cm) was used for deposition of the Cu^{II}-GA/CySA coatings. Briefly, the NO catalytically produced by Cu^{II}-GA/CySA coated PVC was purged from the test solution, which consisted of PBS containing NO donor S-nitrosoglutathione (GSNO, one of the most typical RSNO species used for this test) and reducing agent glutathione (GSH), and was transported to the NO analyzer with a stream of N_2 (g). The amount of NO induced by different samples was determined according to the calibration curves of the NOA reported in details elsewhere.[27-28] To investigate the long-term catalytic effect of the Cu^{II}-GA/CySA coatings, the coated PVC substrates were immersed in NO donor solution, which was replaced every 12 hours at 37°C. Then, the NO donor treated samples were used for testing catalytic NO generation. Also, XPS measurement were adopted to analyze the changes of the surface chemical compositions of theses NO donor-treated samples.

Platelet adhesion and activation

Platelet rich plasma (PRP) was obtained by centrifuging (1500 rpm, 15 min) fresh human whole blood, acquired from the central blood station of Chengdu, China. The blood was treated with tri-sodium citrate in a volumetric ratio of 9:1. Due to the chemical instability of PRP, we added an extra NO donor (10μM GSNO, 10μM GSH) to perform a comparison analysis. Then, we added 1mL of PRP, with or without NO donor, to the surface of each specimen and incubated them for 2 hours. During incubation, the same amount of the NO donor was added to the NO donor group every 30 min. Then, we washed the specimens with saline and immersed them in 2.5% glutaraldehyde overnight. Following further dehydration, we sputtered gold onto the samples and examined them with SEM (Quanta 200, FEI, Netherlands).[29]

Hemolysis evaluation

The sample was firstly placed in a 15 mL centrifuge tube with 9.8 mL saline. An equal amount of saline and distilled water without sample were set as negative and positive control, respectively. Then, 2 mL of the fresh blood was diluted with 2.5 mL of saline. After that, we added 200 μL of the diluted blood into each tube and placed them into the incubator at 37°C for an hour. Finally, each of the incubated blood samples were centrifuged at 3000 r/min for 5 min. In order to find the absorbency of cells that go through, the supernatant was tested with a microplate reader at 540 nm. We followed the equation below to caculate the hemolysis ratio:

$$R=(A_X - A_{NC})/(A_{PC} - A_{NC}) \times 100\%$$

In the equation, A_X, A_{NC} and A_{PC} are the absorbance of the tested sample, the negative control and the positive control, respectively. All of the tests were performed at least twice.

Cell viability assays

In this work, we determined the biocompatibility of the Cu^{II}-GA/CySA coatings using human umbilical vein endothelial cells (HUVECs). We analyzed the HUVEC morphology with actin immunostaining and measured cell proliferation with Cell Counting Kit-8 (CCK-8), with 1 and 3 days of cell culture time. The detailed processes of cell culture are described elsewhere.[29]

Bactericidal assays

Bactericidal activities of the Cu^{II}-GA/CySA coatings were performed in accordance with ISO22196-2011.[30] Both gram-positive *Staphylococcus aureus* (*S. aureus*), strain ATCC 6538, and gram negative *Escherichia coli* (*E. coli*), strain ATCC 25922, were chosen for bacteria test. They were pre-cultured and diluted with either 1/500 (for *E. coli*) or 1/100 (for *S. aureus*) nutrient broth to obtain a test inoculum at a concentration of 6×10^5 bacterium/mL. The planar PVC substrates (25 mm × 25 mm) before and after coating with Cu^{II}-GA/CySA were UV-sterilized. Using a pipet, 0.1mL of the test inoculum was placed onto the substrate surface. They were then covered with a piece of 20 mm × 20 mm film (0.05 to 0.10 mm thick, made of polyethylene, polypropylene or poly (ethylene terephthalate)) and incubated at 35 ± 1°C at a humidity of no less than 90 % for 24 hours. The following formula shows the calculation of the antibacterial rate:

$$R = (N_C - N)/N_C \times 100\%$$

In the formula, R represents the antibacterial rate, N_C and N represent the numbers of the colonies on the control sample and the coated sample, respectively.

Ex-vivo blood circulation thrombogenicity test

We followed all ethical guidelines in accordance with the animal use protocol of China Council on Animal Care and Southwest Jiaotong University. Prior to conducting the experiment, general anesthesia was administered to all experimental animals.We used six New Zealand white rabbits (2.5-3.5 kg) in this experiment. We first isolated the left carotid artery and the right jugular vein of the rabbits, and then cannulated them with an arteriovenous (AV)extracorporeal circuit (ECC). The ECC was unclamped from both sides to allow blood to flow through for 2 hours. Photographs of the cross sections and residual thrombosis of the tubes were taken to analyze the percent occlusion of the circuits. We then, we rinsed the specimens with PBS (pH 7.4) and kept them in 2.5% glutaroladehyde solution (with PBS) overnight. Finally, we dehydrated and performed critical point drying to the specimens for SEM applications.[26,31]

Statistical analysis

We expressed all quantitate results as mean ± standard deviation (SD). With the use of SPSS software, we compared all data with one-way analysis of variance (ANOVA) to evaluate the statistical significance; we considered probability values less than 0.05 as

statistically significant.

3. Results and discussion

Characterization of the Cu^{II}-GA/CySA coatings

To test the feasibility of metal-phenolic surface functionalization strategy, a mixture solution consisting of $CuCl_2 \cdot 2H_2O$ (40 μg/mL), a plant polyphenol GA (0.5 mg/mL) and CySA (0.6 mg/mL) was first employed on the PVC tubing. After 12 hours of dip-coating, the coated tubing exhibited the dark-brown color of polyphenoles (Fig. 2A), suggesting the formation of the coatings onto the PVC tubing. To fabricate the Cu^{II}-GA/CySA coatings with adjustable and controllable content of copper, various feed concentrations of $CuCl_2 \cdot 2H_2O$ ranging from 0 to 60 μg/mL were explored, meanwhile GA and CySA kept at a constant concentration of 0.5 mg/mL and 0.6 mg/mL, respectively. The successful formation of surface coatings on PVC (Fig. S1) as well as silicon (Fig. 2B) were also confirmed by SEM and ellipsometry, respectively. With the use of XPS, analysis showed that the atomic concentration of copper was a function of the feed concentration of $CuCl_2 \cdot 2H_2O$ (Fig. 2C and D), suggesting the robust control of Cu^{II}-GA/CySA surface chemistry at ion/molecular level for engineering PVC.

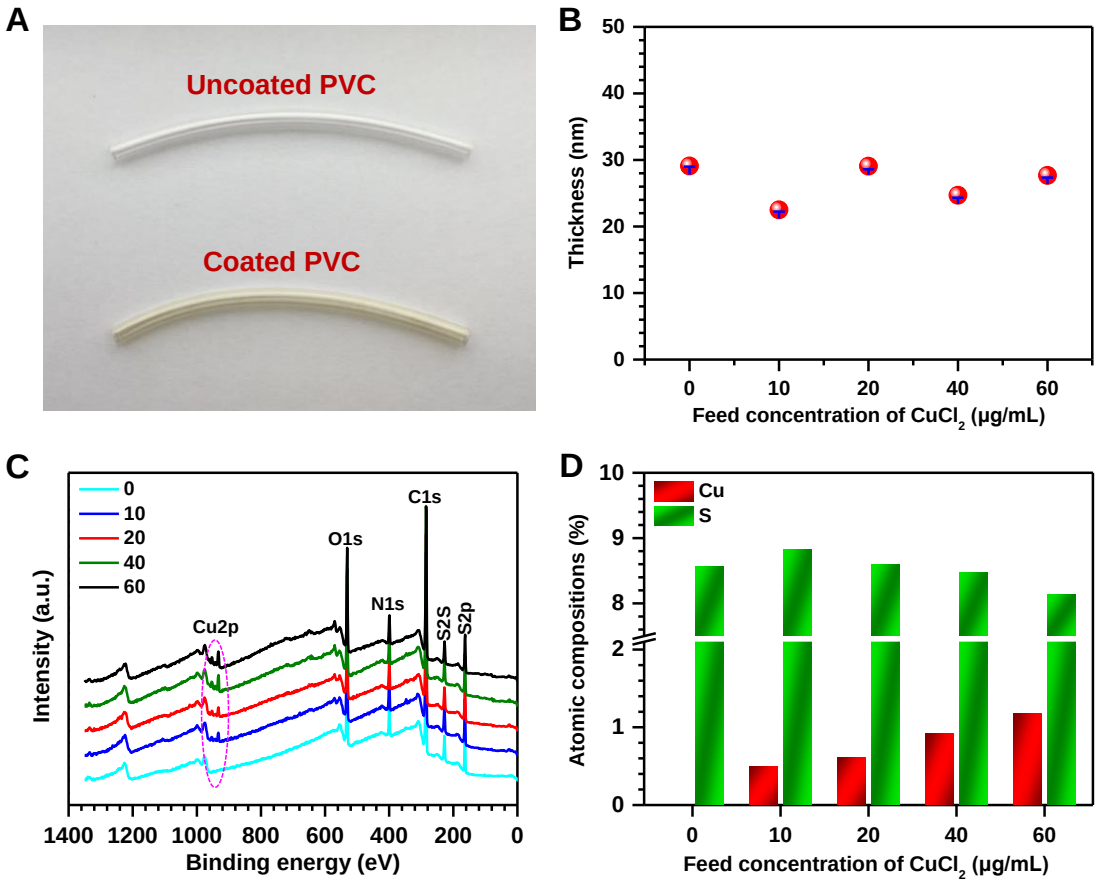

Fig. 2 (A) Photographs of PVC catheter before and after coating with Cu^{II}-GA/CySA. (B) Thickness of the Cu^{II}-GA/CySA coating on the silicon surface as a function of $CuCl_2 \cdot 2H_2O$ feed concentration. (C) XPS spectra of the Cu^{II}-GA/CySA coatings prepared with different feed concentrations of $CuCl_2 \cdot 2H_2O$ ranging from 0 to 60 μg/mL. (D) Shift of Cu and S atomic compositions of the Cu^{II}-GA/CySA coatings fabricated with different feed concentration of $CuCl_2 \cdot 2H_2O$.

To understand the formation mechanism of the Cu^{II}-GA/CySA coatings, surface analysis using GATR-FTIR and high-resolution O1s spectra of the XPS was carried out. As shown in Fig. S2, two new peaks assigned to Cu-O stretching were detected at 540 and 619 cm^{-1}, indicating the chelation of the copper ion by the phenolic oxygens of GA. Meanwhile, the peaks at 3280 and 3370 cm^{-1} assigned to O-H stretching of Ph-OH were largely attenuated. There is a broad peak around the 1600 cm^{-1} in the spectra of the Cu^{II}-GA/CySA coatings, indicating the reinforcement of C=N stretching, ascribed to the Schiff-base reaction induced by the primary amine group of the CySA and the GA. The chemistry of the GA-copper ion coordination, Michael addition and Schiff-base

formation between the primary amine and the gallol groups were further verified using high-resolution O1s spectra of XPS, EPR and MALDI- MS spectra. The high-resolution O1s spectra revealed that the chemical component of the peak being assigned as O-Cu and COO^- at ~ 530 eV of the Cu^{II}(40) coating significantly increased as compared to the Cu^{II}(0) coating (Fig. S3). The formation of Cu^{II}-GA coordination in the Cu^{II}(40) coating was confirmed by the Cu^{II}-GA signals at ~ 3460 mT in EPR spectra (Fig. 3A) and the tris Cu^{II}-GA coordination complex at 569 m/z in MALDI-MS (Fig. 3B). The peak of $[M+H]^+$ ion at 719 m/z demonstrates the role of CySA in cross-linking the tris Cu^{II}-GA coordination complex. We also found that the peaks of $[M+H]^+$ ions at 302, 320 and 489 m/z were clearly present in the MS spectrum of the Cu^{II}(40) coating (Fig. 3B), confirming the crosslinking reactions between the CySA and GA based on Schiff-base and Michael addition reactions (Fig. 3C).

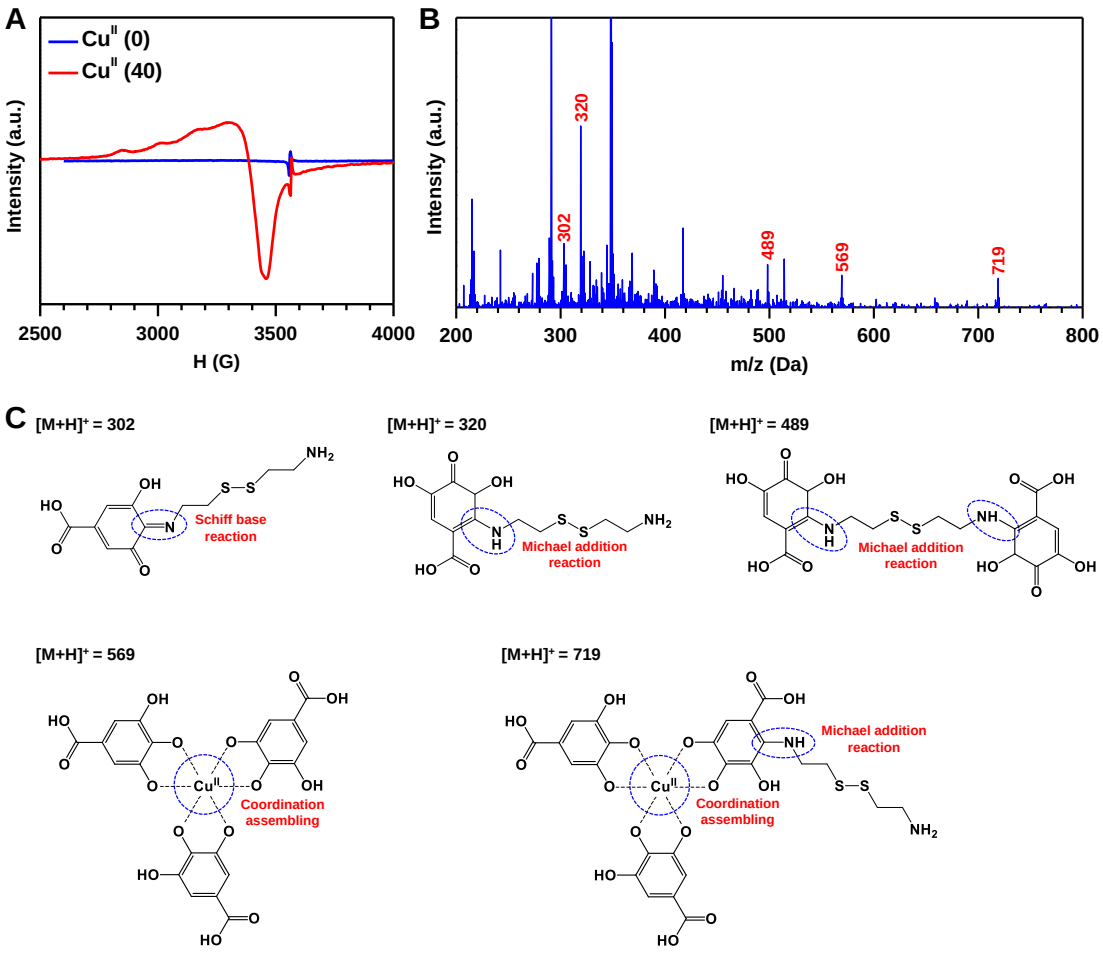

Fig. 3 EPR spectra and MALDI MS analysis of the Cu^{II}-GA/CySA coatings. (A) EPR spectra of Cu^{II}(0)- and Cu^{II}(40)-GA/CySA coatings. (B) MALDI-MS spectra of

Cu^{II}(40) coating. (C) The possible molecule/ion co-assembly manner among the GA, Cu^{2+} and CySA based on EPR and MALDI-MS analysis.

We used real-time chemiluminescent assay to evaluate the *in vitro* catalytic generation of NO from Cu^{II}-GA/CySA coated PVC surface in deoxygenated NO donor solution (pH 7.4), consisting of 10 μM GSNO and 10 μM GSH. The real-time monitoring of the NO production patterns revealed the stable release of NO from the Cu^{II}-GA/CySA coatings (Fig. 4A). This indicates a robust chelation of Cu^{2+} to Cu^{II}-GA/CySA network. More importantly, Cu chelation exhibited a dose-dependent manner, which was supported by the release rates of NO produced by Cu^{II}-GA/CySA coatings (Fig. 4B), confirming the successful formation of the metal-phenolic surface coating for Cu chelation. We also found that the steady NO release rate of Cu^{II}-GA/CySA coatings was a function of the feed concentration of $CuCl_2 \cdot 2H_2O$ and reached a value of up to ~ 18×10^{-10} mol cm^{-2} min^{-1} when 60 μg/mL of $CuCl_2 \cdot 2H_2O$ was used for coating preparation. Additionally, the Cu^{II}-GA/CySA coatings, the Cu^{II}(40) coating in particular, exhibited excellent retention of NO catalytic activity. After a continuous exposure to the NO donor solution for 30 days, it is worth noting that the Cu^{II}(40) coating maintained ~ 51% of release rate of NO generated by a native Cu^{II}(40) coating (Fig. 4C) owing to the good preservation of Cu content within the coating (Fig. 4D). Such good preservation of Cu and the resulting NO catalytic activity imply a promising application in long-term indwelling biomedical devices.

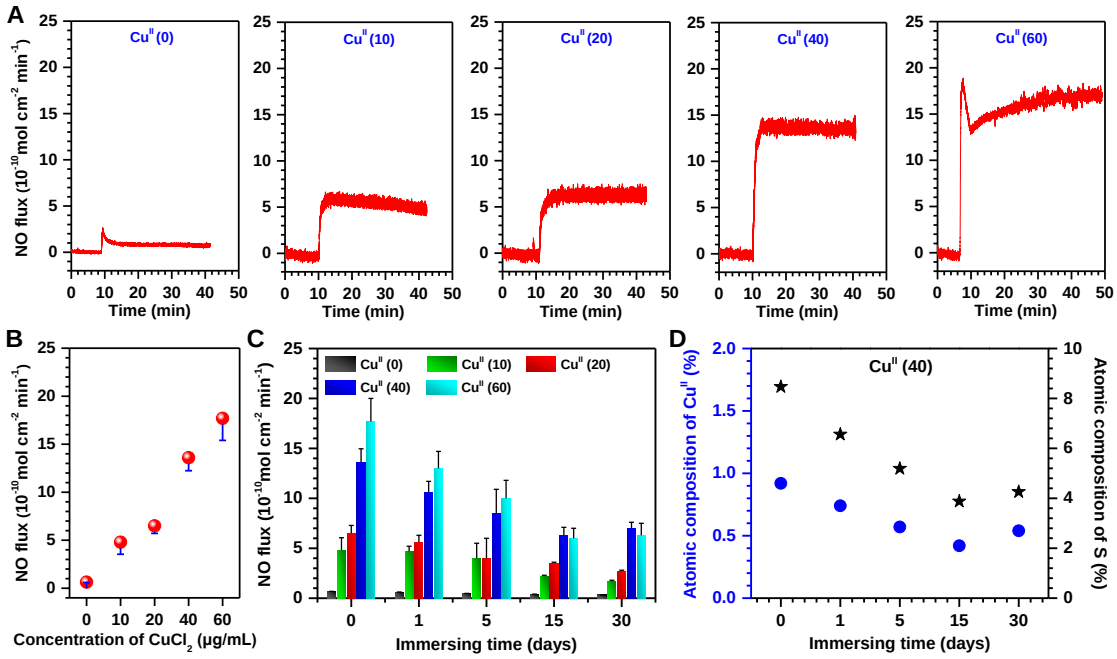

Fig. 4 (A) NO catalytic generation patterns induced by Cu^{II}-GA/CySA coated PVC substrates from deoxygenated PBS (pH 7.4) containing 10 μM GSNO, and 10 μM GSH at 37°C. (B) The influences of the content of Cu^{2+} in the Cu^{II}-GA/CySA coatings on NO release rate. (C) NO release from Cu^{II}-GA/CySA coatings after exposure to the NO donor solution consisting of 10 μM GSNO and 10 μM GSH for up to 30 days, rated to initial as 100%. Such Cu^{II} coatings were prepared with different feed concentration of $CuCl_2 \cdot 2H_2O$ ranging from 0 to 60 μg/mL. (D) Atomic compositions of Cu (blue) and S (black) retained on the surface of Cu^{II}(40) coating after inmmersion into NO donor for up to 30 days. The NO donor solution was replaced every 12 hours. Atomic compositions of the coatings were determined by XPS. Data presented as mean ± SD (n = 4).

Reduced adhesion and activation of platelets *in vitro*

NO is essential in preventing thrombosis as it inhibits platelet adhesion/activation[27,32] through up-regulating the expression of cyclic guanylate monophosphate (cGMP)[33-36]. In order to verify the biological effects of the Cu^{II}-GA/CySA coatings on platelets, the evaluations on the platelet adhesion *in vitro* and the cGMP synthesis were performed. In view of short half-lives of most endogenous RSNO species and the resultant deficiency of RSNOs existed in PRP, the PRP supplemented with rational GSNO (one of the most typical endogenous RSNO species) was used for the *in vitro* platelet assay.

The concentration of cGMP synthesized by platelets incubated with uncoated and Cu^{II}-GA/CySA coated PVC for 2 hours revealed that there was no significant difference among all surfaces in the group without supplement of NO donor, whereas the addition of NO donor in PRP led to a remarkable increase in the cGMP concentration (Fig. S4). The resulting demonstrated the potent catalytic activity of the Cu^{II}-GA/CySA coatings for NO formation and the resulting physiological effects of NO. Upon further investigation, it was also found that the cGMP synthesis in the groups of Cu^{II}-GA/CySA coatings became augmented with the increase of catalytic NO release. The biological activity of cGMP formation was confirmed by analyzing platelet adhesion with the use of SEM. In the group without the NO donor, platelets on all surfaces were severely activated, presented in a full spreading state (Fig. 5A). After supplement of the NO donor, the Cu^{II}-GA/CySA coated surfaces showed the impressive inhibition in the platelet adhesion/activation. Although some platelets were observed on their surfaces, most platelets remained in a resting, nonactivated state. Especially, coating PVC with Cu^{II}(40) and Cu^{II}(60) reduced platelet adhesion and activation by approximately 17- and 38-fold respectively, as compared to the uncoated PVC (Fig. 5B and C).

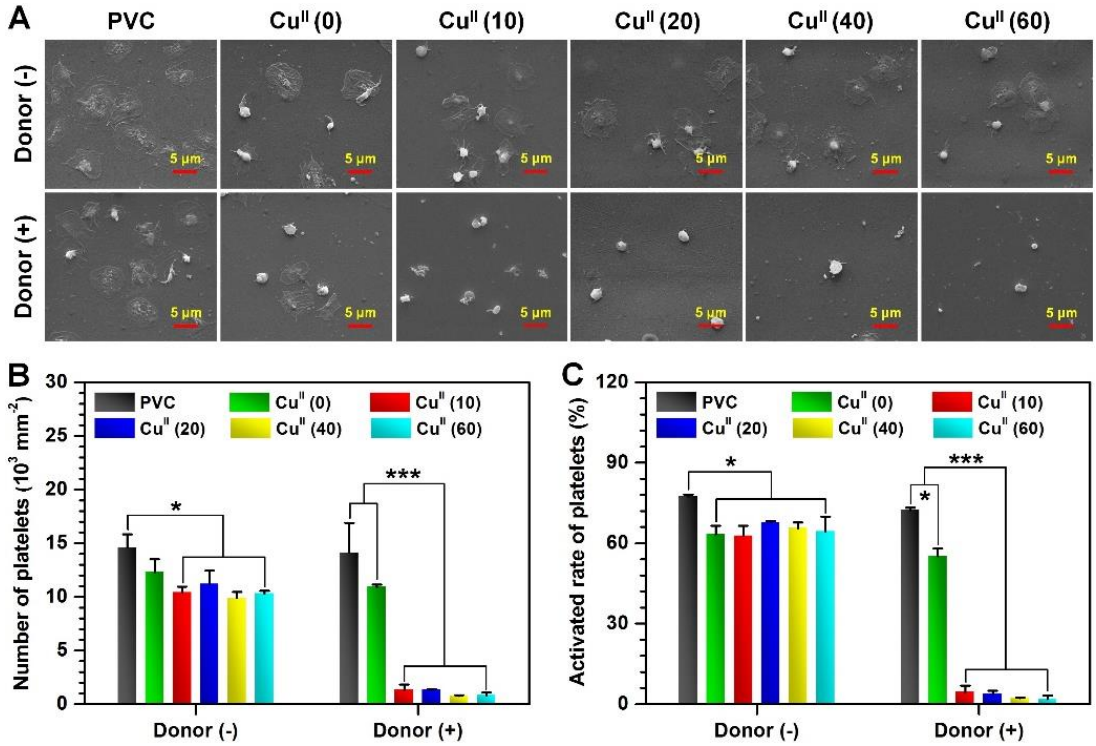

Fig. 5 (A) Representative SEM images of *in vitro* platelet adhesion. Statistical results of (B) the number and (C) the activated rate of platelets incubated with uncoated and

Cu^{II}-GA/CySA coated PVC for 2 hours. Data presented as mean ± SD and analyzed using a one-way ANOVA, *p < 0.05, ***p < 0.001.

Hemolysis and cytotoxicity test

A hemocompatible blood-contacting material should not induce activation of coagulation factors, platelet adhesion/activation and hemolysis. We thereby performed a hemolysis ratio test of our new synthesized material of Cu^{II}-GA/CySA. The hemolysis ratios of the Cu^{II}-GA/CySA-coated PVC revealed that their values were all within 1% (Table S1), and were far below the accepted threshold value of 5%,[37] suggesting that these coatings have good hemocompatibility. Additionally, as a coating used for blood-contacting indwelling biomedical devices (such as central venous catheter), it is inevitable to come into contact with endothelium of blood vessel. Therefore, evaluation of cytotoxicity via endothelia cells (ECs) was necessary. Cell Counting Kit-8 (CCK-8) was used for investigating the cytotoxicity of the Cu^{II}-GA/CySA coatings (Fig. S5). Our results revealed that the Cu^{II}-GA/CySA coatings enhanced proliferation of ECs, indicating an excellent biocompatibility of the Cu^{II}-GA/CySA coatings, implying it to be a promising platform for the engineering of blood-contacting devices.

Antibacterial properties of the Cu^{II}-GA/CySA coating

Given the efficient anticoagulation and excellent biocompatibility of the Cu^{II}-GA/CySA coatings *in vitro*, we explored whether such metal-phenolic surface functionalization strategy could combat bacteria. In this study, we chose the representative bacterium, namely *E. coli* and *S. Aureus*, as they are the are gram-negative and gram-positive bacterium respectively, and also are the most prevalent species of bacterium with regards to the development of stent graft infections.[38,39] These results revealed that coating the PVC with Cu^{II}-GA/CySA led to effective suppression of both *E. coli* and *S. aureus* (Fig. 6 and Fig. S6 and Table S2). The antibacterial effect was strongly dependent on the content of Cu^{II} in the Cu^{II}-GA/CySA coatings, the antibacterial rate reached a value of up to 99% when the feed concentration of $CuCl_2 \cdot 2H_2O$ increased to 20 μg/mL (Fig. 6A and B).

Taken into consideration of the NO catalytic behavior, retention of Cu content, *in vitro* platelet adhesion, hemolysis ratio, cytotoxicy and antibacterial properties of the

Cu^{II}-GA/CySA coatings together, these results confirmed that 40 μg/mL is the optimal feed concentration of $CuCl_2 \cdot 2H_2O$ to form the Cu^{II}-GA/CySA coating. To evaluate the durability of antibacterial effect of the Cu^{II}-GA/CySA coating, before this study, the Cu^{II}(40)-modified PVC was continuously immersed into NO donor for 1, 5, 15 and 30 days. As shown in Fig. 6C, the Cu^{II}(40)-modified PVC after continuous treatment by PBS containing NO donor up to 30 days still exhibited ~ 99% antibacterial rate, suggesting the possibility for long-term clinical application.

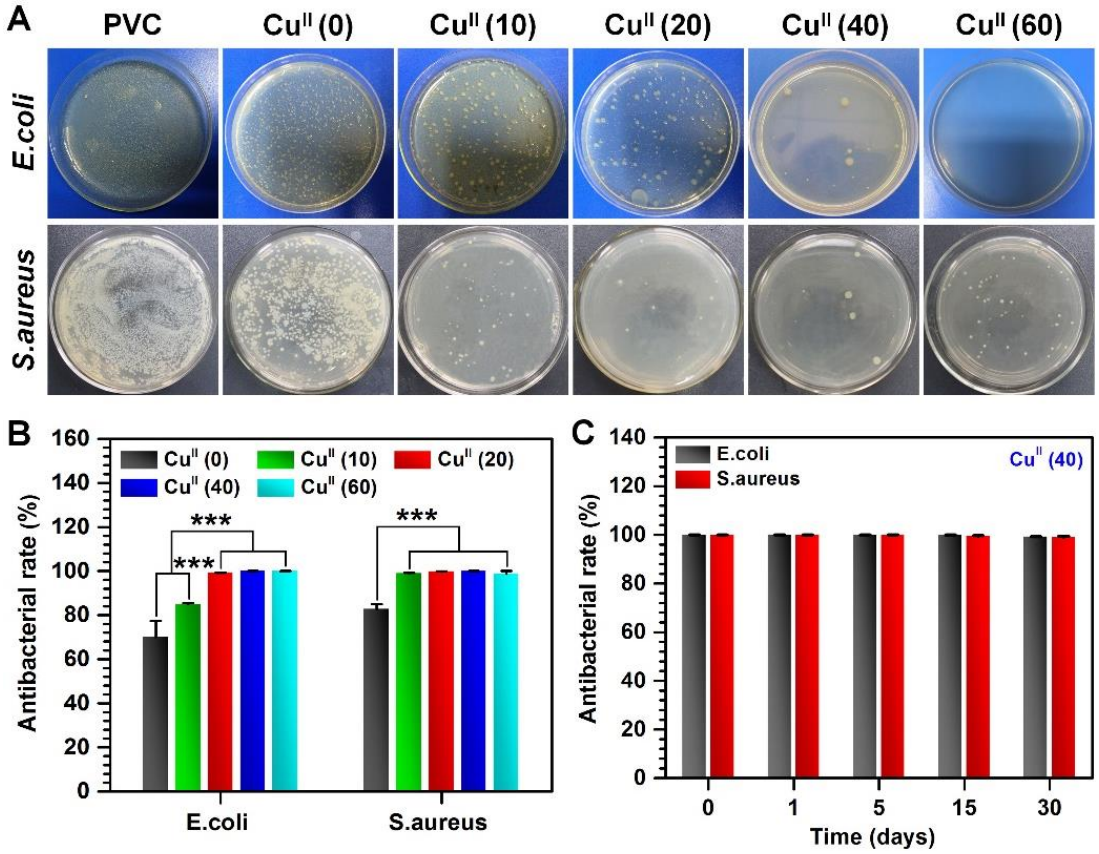

Fig. 6 (A) Representative photographs of colonization by *E. coli* and *S. aureus* on the PVC substrates before and after modification by the Cu^{II}-GA/CySA coatings. (B) Statistical results of the antibacterial rates of different Cu^{II}-GA/CySA coatings against *E. coli* and *S. aureus*. (C) Antibacterial rate of Cu^{II}(40)-coated PVC against *E. coli* and *S. aureus* after continuous exposure to the NO donor consisting of 10 μM GSNO and 10 μM GSH for up to 30 days; the good retention of antibacterial effects of Cu^{II}(40)-coated PVC after continuous exposure to PBS containing NO donor reveals excellent stability of the Cu^{II}(40) coatings and sufficient dose of Cu^{II} retained in the Cu^{II}(40)

coatings. The NO donor solutions were replaced every 12 hours. Data presented as mean ± SD and analyzed using a one-way ANOVA, ***$p < 0.001$.

Reduced thrombosis *in vivo*

To examine the antithrombogenic properties of Cu^{II}-GA/CySA modified PVC, an *ex vivo* perfusion experiment without any systemic heparin anticoagulation was performed. We assembled the unmodified and Cu^{II}(40) modified commercially available PVC tubes into an AV shunt as shown in Fig. 7A. The abilities of the Cu^{II}-GA/CySA coatings to prevent thrombosis and support patency of circuit and blood flow in a New Zealand rabbit AV shunt model were then evaluated. In this study, to investigate the long-term anti-thrombogenic effect of the Cu^{II}(40)-coated PVC tubes, these tubes were immersed in NO donor solution replaced every 12 hours for 30 days (marked as Cu^{II}(40)-30 days) for antithrombogenic test.

The condition of 2 hours' *ex-vivo* circulation in the AV shunts with systemic supplement of NO donor revealed that the circuit of uncoated PVC presented complete occlusion, whereas the circuit coated with Cu^{II}(40) showed no detectable occlusion (Fig. 7B and C). Despite the detectable occlusion in the group of Cu^{II}(40)-30 days, it had only 3.4 ± 0.2% occlusion (the cross-section diameter of tubing was used for assessing the occlusion) (Fig. 7D). Evaluation of thrombus harvested from the circuits after 2 hours of circulation revealed that both Cu^{II}(40) and Cu^{II}(40)-30 days-functionalized groups presented a significant decrease in occlusive thrombosis. Total thrombus weights in Cu^{II}(40) and Cu^{II}(40)-30 days-coated circuits were reduced from 399.1 ± 49.4 mg in uncoated PVC to 30.4 ± 12.0 and 66.4 ± 8.8 mg, respectively (Fig. 7E). SEM analysis revealed that both Cu^{II}(40) and Cu^{II}(40)-30 days-functionalized PVC and impressively prevented the formation of thrombus on their surfaces (Fig. 7F). On the internal surface of uncoated PVC tubing, severe thrombus was observed, whereas only a few scattered non-activated platelets were found on the Cu^{II}(40)-coated PVC. Although a small amount of thrombus was detected in the Cu^{II}(40)-30 days-modified PVC tubing, the vast majority of area was free of blood clots, suggesting that it also possessed excellent antithrombogenic properties. In addition, as the undisturbed blood flow in the implanted tubing lumen plays a vital role in hemocompatibility, the testing

blood flow rates in the PVC tubing circuits after 2 hours of circulation was further performed. As shown in Fig. 7G, both of Cu^{II}(40)- and Cu^{II}(40)-30 days-modified PVC tubing retained 88.2 ± 4.1 and 78.7 ± 3.1 % of the initial blood flow rate respectively, which were much higher than 18.6 ± 6.6 % in the group of unmodified PVC tubing. The good retention of antithrombogenic effects of Cu^{II}(40)-coated PVC was attributed to the good retention of Cu^{II} in the coatings after continuous immersion into NO donor solution, demonstrating the long-term thromboprotective property.

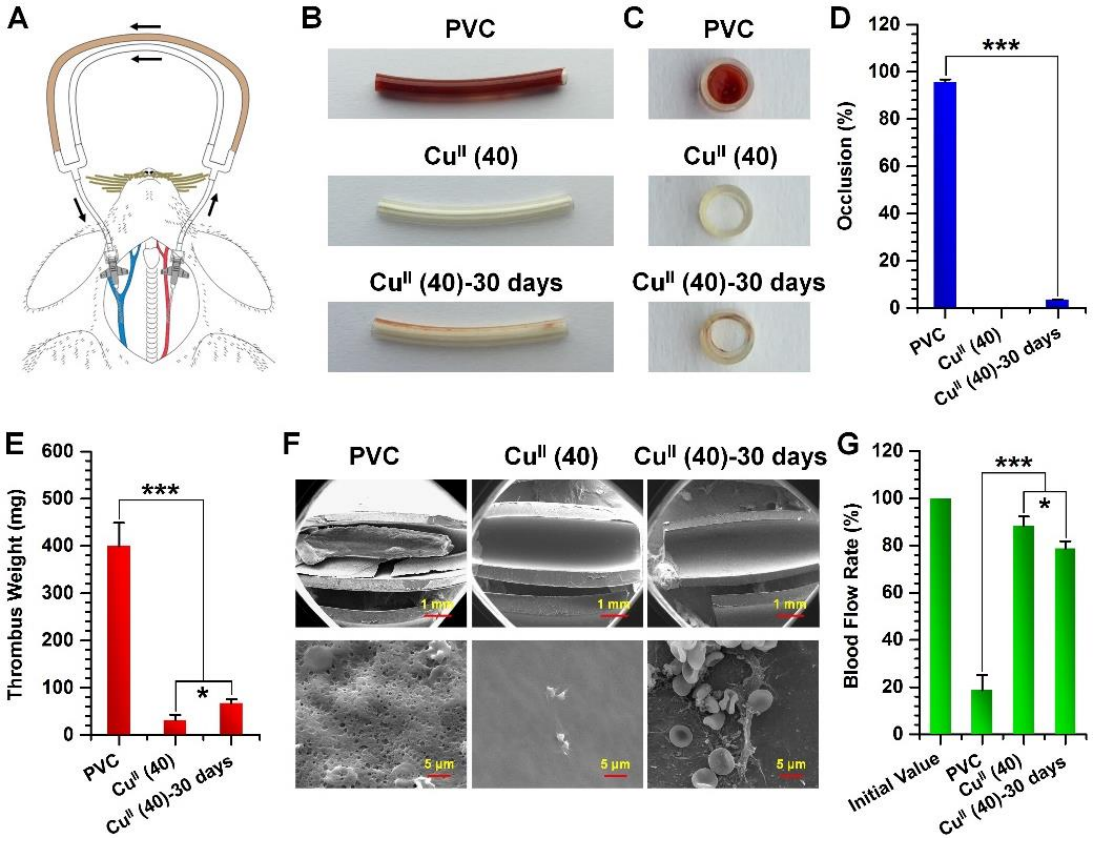

Fig. 7 (A) Scheme of the New Zealand white rabbit AV shunt model exhibiting placement of the cannulae in the carotid artery and jugular vein connected by PVC tubing. The direction of blood driven by the hear is indicated by black. (B) Photographs and (C) cross sectional photographs of the bare, Cu^{II}(40)-coated and Cu^{II}(40)-30 days-coated PVC tubings. (D) Percent occlusion of the PVC tubing before and after modification by the Cu^{II}(40) coating. (E) Statistical results of thrombus weight formed on PVC tubings before and after modification by Cu^{II}(40) coating. (F) SEM images of the inwalls of the PVC tubings after 2 hours of circulation. (G) Blood flow rates in

different PVC tubing circuits at the end of circulation experiments. Data presented as mean ± SD and analyzed using a one-way ANOVA, *$p < 0.05$, ***$p < 0.001$.

4. Conclusions

In summary, we have developed a straightforward and universal strategy to fabricate a novel dual functional coating with the metal-phenolic-amine network, which could confer the vascular devices with the properties of long-term antithrombosis and antibacteria. These specific functionalities were realized by the incorporation of the Cu^{II} ions into the metal-phenolic-amine network based on simple ion/molecule co-assembly of Cu^{II}, GA and CySA. The Cu^{II} ions in the resulting coatings do not only allow the modified surfaces to be bacterial resistant, but also catalytically generate NO from endogenous RSNO in blood to prevent platelet adhesion/activation, and impressively reduce thrombosis *in vivo*. As the durable metal-phenolic-amine network provides the resultant coating with excellent stability, it retains the properties of antibacterial and antithrombogenic effects over a long term period. We envison that such copper-phenolic-amine surface functionalization strategy can serve as a propitious and functional solution to the complications of indwelled blood-contacting biomedical devices in clinical practices.

Conflicts of interest

There are no conflicts to declare.

Acknowledgements

This work was supported by the National Natural Science Foundation of China (Project Key Program 81330031, 31570957 and 81501596), Distinguished Young Scholars of Sichuan Province (Project 2016JQ0027) the Fundamental Research Funds for the Central Universities (Project 2682018ZT23) and the start-up fund (1-ZE7S) and central research fund (G-YBWS) from the Hong Kong Polytechnic University.

References

1. B. Furie and B. C. Furie, *N. Engl. J. Med.*, 2008, **359**, 938-949.
2. E. A. Vogler and C. A. Siedlecki, *Biomaterials*, 2009, **30**, 1857-1869.
3. S. Li and J. J. Henry, *Annu. Rev. Biomed. Eng.*, 2011, **13**, 451-475.
4. R. C. Moellering Jr, *Journal of antimicrobial chemotherapy*, 2011, **67**, 4-11.
5. B. Allegranzi, S. B. Nejad, C. Combescure, W. Graafmans, H. Attar, L. Donaldson and D. Pittet, *Lancet*, 2011, **377**, 228-241.
6. G. Conn, A. G. Kidane, G. Punshon, R. Y. Kannan, G. Hamilton and A. M. Seifalian, *Expert. Rev. Med. Devices*, 2006, **3**, 245-261.
7. J. Aw, F. Widjaja, Y. Ding, J. Mu, Y. Liang and B. Xing, *Chem. Commun.*, 2017, **53**, 3330-3333.
8. H. Ji, H. Sun and X. Qu, *Adv. Drug Deliv. Rev.*, 2016, **105**, 176-189.
9. M. P. Pai, R.C. Mercier and S. A. Koster, *Ann, Pharmacother.*, 2006, **40**, 224-228.
10. M. de Hoog, J. W. Mouton and J. N. van den Anker, *Clin Pharmacokinet.*, 2004, **43**, 417-440.
11. I. Banerjee, R. C. Pangule and R. S. Kane, *Adv. Mater.*, 2011, **23**, 690-718.
12. S. Jiang and Z. Cao, *Adv. Mater.*, 2010, **22**, 920-932.
13. H. P. Felgueiras, L. Wang, K. Ren, M. Querido, Q. Jin, M. Barbosa, J. Ji and M. Martins, *ACS Appl. Mater. Interfaces*, 2017, **9**, 7979-7989.
14. T. Sun, H. Tan, D. Han, Q. Fu and L. Jiang, *Small*, 2005, **1**, 959-963.
15. D. C. Leslie, A. Waterhouse, J. B. Berthet, T. M. Valentin, A. L. Watters, A. Jain, P. Kim, B. D. Hatton, A. Nedder and K. Donovan, *Nat. Biotechnol.*, 2014, **32**, 1134-1140.
16. N. Holten-Andersen, T. E. Mates, M. S. Toprak, G. D. Stucky, F. W. Zok and J. H. Waite, *Langmuir*, 2008, **25**, 3323-3326.
17. H. Ejima, J. J. Richardson, K. Liang, J. P. Best, M. P. van Koeverden, G. K. Such, J. Cui and F. Caruso, *Science*, 2013, **341**, 154-157.
18. H. Ejima, J. J. Richardson and F. Caruso, *Nano Today*, 2017, **12**, 136-148.
19. R. Pashley, *Adv. Colloid. Interface Sci.*, 1982, **16**, 57-62.
20. J. N. Israelachvili, in *Intermolecular and Surface Forces, ed.* J. N. Israelachvili, Academic Press, Boston, Third Edition, 2011, **15**, 341-380.
21. G. P. Maier, M. V. Rapp, J. H. Waite, J. N. Israelachvili and A. Butler, *Science*, 2015, **349**, 628-632.
22. G. Grass, C. Rensing and M. Solioz, *Appl. Environ. Microbiol.*, 2011, **77**, 1541-1547.
23. G. Kirakosyan, K. Trchounian, Z. Vardanyan and A. Trchounian, *Cell Biochem. Biophys.*, 2008, **51**, 45-50.
24. M. K. Ballo, S. Rtimi, S. Mancini, J. Kiwi, C. Pulgarin, J. M. Entenza and A. Bizzini, *Appl. Microbiol. Biotechnol.*, 2016, **100**, 5945-5953.
25. S. Hwang, W. Cha and M. E. Meyerhoff, *Angew. Chem.*, 2006, **118**, 2811-2814.

26. Z. Yang, Y. Yang, L. Zhang, K. Xiong, X. Li, F. Zhang, J. Wang, X. Zhao and N. Huang, *Biomaterials*, 2018, **178**, 1-10.
27. P. N. Coneski and M. H. Schoenfisch, *Chem. Soc. Rev.*, 2012, **41**, 3753-3758.
28. Z. Yang, Y. Yang, K. Xiong, X. Li, P. Qi, Q. Tu, F. Jing, Y. Weng, J. Wang and N. Huang, *Biomaterials*, 2015, **63**, 80-92.
29. Z. Yang, Q. Tu, M. F. Maitz, S. Zhou, J. Wang and N. Huang, *Biomaterials*, 2012, **33**, 7959-7971.
30. B.E. ISO, 22196. Measurement of antibacterial activity on plastics and other nonporous surfaces, Geneva: International Organization for Standardization, 2011.
31. X. Li, H. Qiu, P. Gao, Y. Yang, Z. Yang and N. Huang, *NPG Asia Mater.*, 2018, **10**, 482-496.
32. C. Moore, C. Tymvios and M. Emerson, *Thromb. Haemost.*, 2010, **104**, 342-349.
33. W. P. Arnold, C. K. Mittal, S. Katsuki and F. Murad, *Proc. Natl. Acad. Sci. U. S. A.*, 1977, **74**, 3203-3207.
34. C. K. Mittal, J. M. Braughler, K. Ichihara and F. Murad, *Biochim. Biophys. Acta*, 1979, **585**, 333-342.
35. F. Murad, *Biosci. Rep.*, 2004, **24**, 452-474.
36. T. Malinski, *Am. J. Cardiol.*, 2005, **96**, 13-24.
37. L. Li, M. Tu, S. Mou and C. Zhou, *Biomaterials*, 2001, **22**, 2595-2599.
38. D.D. Bannerman, M.J. Paape, J.W. Lee, X. Zhao, J.C. Hope, P. Rainard, *Clin. Diagn. Lab. Immunol.*, 2004, **463**, 463-472
39. C. Setacci, E. Chisci, F. Setacci, L. Ercolini, G.D. Donato, N. Trois, G. Galzerano, S. Michelagnoli, *Aorta*, 2014, **256**, 255-264